Suppressing the formation of high *n*-phase and 3D perovskite in the fabrication of Ruddlesden-Popper perovskite thin films by bulky organic cation engineering

Rubén Vázquez-Cárdenas,[a,b] Jesús Rodríguez-Romero,[a,c]* Carlos Echeverría-Arrondo,[a] Jesús Sanchez-Diaz,[a] Vladimir S. Chirvony,[d] Juan P. Martínez-Pastor,[d] Pedro Díaz-Leyva,[e] Juan Reyes-Gómez,[f] Isaac Zarazua,[g] and Iván Mora-Seró[a]*

[a] Institute of Advanced Materials (INAM), Universitat Jaume I, Av. Sos Baynat, s/n, 12071 Castelló, Spain.

[b] Facultad de Ciencias Químicas, Universidad de Colima, Km 9 Carretera Colima-Coquimatlán, Coquimatlán, Colima, C.P. 28400, Mexico.

[c] Facultad de Química, Universidad Nacional Autónoma de México. Circuito Exterior s/n, C.U., Coyoacán, 04510 Mexico City, Mexico.

[d] UMDO, Instituto de Ciencia de los Materiales, Universidad de Valencia, c/Catedrático J. Beltrán, 2, Paterna 46980, Spain.

[e] Departamento de Física, Universidad Autónoma Metropolitana Iztapalapa, San Rafael Atlixco 186, 09340 Mexico City, Mexico.

[f] Facultad de Ciencias, Universidad de Colima, Colima, Colima 28045, Mexico.

[g] Universidad de Guadalajara, Centro Universitario de los Lagos. Lagos de Moreno, Jalisco C.P. 47463, Mexico.

*e-mails: jrr@quimica.unam.mx; sero@uji.es

Abstract

Two dimensional perovskites (2D PVKs) were first studied because of their dielectric and magnetic properties for dielectric and transistor application in electronic field. As the optical properties were elucidated with the change of *n* in function of the organic and metal component, their fundamental features such as exciton binding energy, quantum and dielectric confinement, higher thermal and moisture resistance allowed them to position as one of the promising materials for a wide and diverse number of applications such as solar cells. However, the preparation of quasi-2D PVKs thin films containing single phase materials corresponding just to the desired *n* value (*n*=number of neighboring inorganic layers in a quasi-2D structure) instead the wide mixture of different *n* and 3D PVK phases, usually obtained, is a very challenging topic to overcome. Until now, a few methods to reach that goal has been proposed, however, they imply the use of additional reagents or fabrication steps, increasing the number of precursor materials and the complexity of the process. Here, we report the fabrication of quasi-2D PVKs thin films with n=2, where the formation of undesired higher-n phases, including 3D PVKs, were effectively reduced without any extra reagent/additive only making use of the particular features of the molecules in each of evaluated formulation. The powder XRD, absorbance and PL spectroscopy, at room and low temperature, reveal the fabrication of thin films with reduced phase polydispersity and the absence of 3D PVK phase. Dynamic light scattering results exhibit that the use of bulky cations possessing robust intermolecular bonding interactions in the precursor solution, promotes the formation of colloidal nanoparticles by diminishing the number

of particles out of the colloidal size. Thus, resulting in the desired higher concentration of low-*n* phases as compared to high-*n* and 3D phases in PVK thin films. A correlation between dynamic light scattering and ^{1}H Nuclear Magnetic Resonance studies at room and high temperatures shows that the stronger the intermolecular interactions between bulky cations and the metal halide (in the precursor solution), the better the control on n-phase polydispersity. Interestingly, despite the potential steric hindrance owing by the large substituents on the main organic chain of the ammonium cation. The feasibility to suppress the formation of large-*n* phase and 3D PVKs during the fabrication of quasi-2D PVKs thin films using a cation with stronger intermolecular interaction without additives or extra fabrication steps will promote an accessible progress of the technology based on this kind of materials.

Introduction

The dielectric and magnetic properties of multilayered 2D systems took the attention of scientific field back in the 80´s.[1-2] There, the first systematic studies of their optical properties were done by Calabrese *et al.* and the "in between" concept was first introduced by the analysis of a whole halide perovskite family series with discrete composition.[3] Then, in the 90´s, the variation in the electrical properties as the series of the n-members changed was demonstrated with the usage of different organic cations and metals in transistor applications.[4-5] Thus demonstrating their potential as semiconductors. Nowadays, two-dimensional perovskites (2D PVKs) represent a class of widely studied materials, [6-7] which have been considered as promising materials for the next generation optoelectronic and photovoltaic devices.[8-11] Initially, 2D PVKs were not considered as promising sensitizers with a real potential in photovoltaics due to several drawbacks such as their limited absorption of the solar spectrum due to their higher band gaps (≈ 2.4 eV),[9] and their stronger exciton binding energies (>150 meV),[12] which are owing to the quantum and dielectric confinement effects observed in layered systems.[13-14] However, the management of those issues through the development of 2D PVKs with partial 3D character,[15] molecular[16-17] and processing engineering,[10, 18-20] but principally due to their intrinsic higher resistance to moisture and higher temperatures than conventional 3D PVKs,[9, 21-22] contributed to their wide applications as an active layer in photovoltaics. In contrast, the high exciton binding energy makes these materials interesting for other optoelectronic applications as LEDs.[23] Structurally, 2D PVKs consist of $[PbI_6]^{4-}$ corner-sharing octahedra sandwiched between insulating barriers

of bulky organic cations (BOCs).[24-26] Theoretically, the desired number of semiconductor layers, referred as <*n*>, could be controlled by the stochiometric relationships between the chemical precursors. However, the fabrication of thin films by solution processing methods with single <*n*> phase, even with just a reduced <*n*> polydispersity, is a very difficult experimental issue that this technology present.

To date, optical properties of 2D PVKs has been widely studied principally for single crystals.[27-28] In contrast with the typical observation of single *n* phase in flakes or single crystals, thin films prepared by solution methods usually exhibit a wide distribution over <*n*>, which implies that the films will contain a complex mixture of QWs with different *n*.[29] This results in the observation of complex and often low-controllable properties. For example, materials formed by mixed *n*-phases will show a set of different energy band gaps, exciton binding energies, carrier´s diffusion lengths, etc., affecting the global performance of the photovoltaic and optoelectronic devices. [30, 31] Therefore, the fabrication of single-phase quasi-2D PVK-based thin films remains as a very timely task.

Recently, Huang *et al*. demonstrated a successful method to obtain single-*n* phase quasi-2D PVKs based thin films through the application of a strong coordinating agent (acetate anion) at the first stage of the fabrication, i.e., in the precursor solution. The authors state that an effective coordinative bonding interaction between the acetate anion and the Pb^{2+} ion controls the final assembly of the layered perovskite by an uniformly distributed intermediate phase with near-monodisperse particles.[32] This discovery agrees with previous observations about the significance that organic moiety has at the coordination step during the organic-

inorganic complex formation in the precursor solution and the quality of the obtained thin films.[33] However, to reach these results it is mandatory the inclusion of additives (e.g. NH_4SCN),[34] which increases the complexity of the experimental process and could also lead to the increase of the cost of the materials.

Here, considering the importance of the chemistry of the precursor solutions, we tackle the problem by a chemical engineering strategy. We evaluate three bulky organic cations (BOCs) for fabrication of nominal $\langle n \rangle = 2$ thin films. The powder X-ray diffraction (*p*XRD) results and optical characterization at room (300K) and low (20K) temperature (RT and LT, respectively) show that when any of the substituted cations is used, a reduced phase polydispersity, i.e., *n* value, is obtained. In contrast, when the thin films were prepared with PEA, the characterization displays a huge concentration of high n-phases and even it is possible to detect 3D perovskite. By Dynamic Light Scattering (DLS) and ^{1}H Nuclear Magnetic Resonance (^{1}H NMR), we determine that the stronger the intermolecular bonding interaction between the BOC and the inorganic sheets, the smaller the size of the colloidal particle in the precursor solution and better the control of polydispersity over *n*. Therefore, we found that the use of cations which induced stronger bonding interactions into the precursor solution will lead to an improved control of phase polydispersity and to the suppression of the 3D PVK phase formation.

Experimental Section

Materials. All reactants were used without further purification. Lead Iodide (PbI_2: 99.999%) was purchased form TCI. Methylammonium iodide (MAI, 98%), Phenylethylammonium iodide (PEAI, 98%), 4-methoxy-phenylethylammonium iodide (MeOPEAI, 98%) and 4-fluoro-phenylethylammonium iodide (FPEAI, 98%) were purchased form GreatCell Solar Materials. Dimethyl sulfoxide (DMSO) and dimethylformamide (DMF) were purchased from Sigma-Aldrich.

Thin film fabrication. Films were fabricated over common glass substrates which were previously clean with soap (Hellmanex) and deionized water, followed by sonication in 1) ethanol, 2) isopropanol and 3) acetone, for 15 minutes each step and then dried with compressed air. The clean substrates were put into UV-O_3 chamber for15 minutes before the deposition procedure. Later, the substrates were pre-heated at 130 °C and moved to the spin-coater without cooling. There, 100 µL of a preheated perovskite precursor solution (100 ºC) were deposited on the substrate and spun at 7000 rpm for 10s. A one-step spin-coating process was used with the hot-casting method. The obtained films were homogeneous and reproducible.

The Ruddlesden-Popper perovskite (2D RPPs) synthesis was focused on the general formula $(R)_2MA_{n-1}Pb_nI_{3n+1}$ to obtain perovskites of the series n=1 and n=2. The precursor solution was prepared from a stoichiometric reaction of an organic bulky cation (PEA, FPEA, MeOPEA or a mixture among them), MAI and PbI_2 by maintaining carefully a ratio of 2:(n- 1):n (see table 1 and 2) in 1mL of DMF and 0.095 mL of DMSO. The first step for preparing the solution is to dissolve the

stoichiometry quantity of the desired bulky cation in the entire volume until it becomes a clear dissolution, then, if needed, MAI is dissolved as second step using the correct stoichiometry quantity for the targeted n. Finally, the amount of PbI_2 mass is added and dissolved until a clear solution is achieved without suspended particles.

Table 1. Mass quantity of the components for <n>=1 thin films.

Sample	PbI_2 (g)	MAI (g)	PEAI (g)	F-PEAI (g)	MeO-PEAI (g)
$(PEA)_2PbI_4$	0.1126	-------	0.1216	-------	-------
$(FPEA)_2PbI_4$	0.1126	-------	-------	0.1304	-------
$(MeOPEA)_2PbI_4$	0.1126	-------	-------	-------	0.1363

Table 2. Mass quantity of the components for <n>=2 thin films.

Sample	PbI_2 (g)	MAI (g)	PEAI (g)	F-PEAI (g)	MeO-PEAI (g)
$(PEA)_2Pb_2I_7$	0.1126	0.0194	0.0608	-------	-------
$(FPEA)_2Pb_2I_7$	0.1126	0.0194	-------	0.06523	-------
$(MeOPEA)2Pb_2I_7$	0.1126	0.0194	-------	-------	0.06816
$(PEA/MeOPEA)_2Pb_2I_7$	0.1126	0.0194	0.0304	-------	0.0340
$(MeOPEA/FPEA)_2Pb_2I_7$	0.1126	0.0194	-------	0.0326	0.0340

Characterization. The X-ray diffraction patterns were carried out using a diffractometer (D8 Advance, Bruker AXS) (Cu Kα, wavelength of l = 1.5406 Å) within the range of 2θ from 3 to 35° with a step size of 0.04º and a counting time of 3s per step. Absorption spectra were recorded with a Varian Cary 300 BIO UV-Vis spectrophotometer in the range of 350-800 nm. Photoluminescence (PL)

measurements were obtained using a Horiba Scientific fluorimeter Fluorolog 3-11. For the PL, the excitation wavelength was λ_{exc} = 420 nm and the detection range within 450-810 nm. PL and absorption measurements of thin films at low-temperature were realized in a closed-cycle He cryostat, which can be cooled down to 15 K. The samples were excited by a 200 fs pulsed Ti:sapphire (Coherent Mira 900D) at a repetition rate of 76 MHz doubled to 405 nm with a BBO crystal. The backscattered PL signal was dispersed by a double 0.3-m focal length grating spectrograph/spectrometer (1200 g/mm with 750 nm blaze) and detected by a Si micro photon device (MPD) and single-photon avalanche diode (SPAD) photodetector (connected through a multimode optical fiber to the monochromator); the SPAD was attached to a time correlated single photon counting electronic board (TCC900 from Edinburgh Instruments). The instrument response function is about 50 ps. For absorption spectra measurements, a xenon lamp was used. Dynamic light scattering (DLS) based sizing was performed with a 3D-LS spectrometer (LS Instruments, Switzerland) equipped with a 632.8 nm laser, a goniometer with moveable detectors (two APDs used in a pseudo-cross correlation mode) and a temperature-controlled index matching bath filled with decalin. The scattering angle was θ = 30°, laser intensity was adjusted to 12.3 mW and temperature was adjusted to 20° C. Measurements of 300 s of duration have been performed on each sample to obtain the intensity auto-correlation function (IACF) and the CONTIN algorithm[35] has been applied to these IACFs using a decay factor of 0.8. ^{1}H Nuclear Magnetic Resonances were acquired in a Varian 400-MR (400 MHz) and Jeol 600ECZR (600 MHz) spectrophotometers.

Theoretical calculations. (a) Determination of the cation´s size. The size of PEA, F-PEA, and MeO-PEA bulky cations was determined with “Quantum Espresso”, a computational tool based on density functional theory (DFT), plane waves, and pseudopotentials.[36] The structures were geometrically relaxed on the Γ point using PBEsol pseudopotentials,[37] and the size of each cation was considered as the distance from the farthest hydrogen atoms in the molecule, see Fig. S1. (b) Determination of the interplanar distance. The distance between the farthest inorganic planes in 2D perovskites (n=1 and n=2) was obtained with “Quantum Espresso”[36] as well. For this purpose, we built up five-unit cells long in the z direction. In the case of PEA, the DFT supercell was extracted from an experimental database (ICSD); for F-PEA, we chose the reported parallel slip-stacked configuration;[38] and for MeO-PEA, two configurations were studied: parallel slip-stacked and edge-to-face stacked. These cells were geometrically relaxed on a Monkhorst-Pack grid of 2 x 2 x 1 k points until the forces on the individual nuclei were smaller than 0.008 Ry/a0. From the calculated total energies, which included spin-orbit interactions, we determined that the edge-to-face stacked configuration was more stable than the parallel slip-stacked configuration, and thus the one adopted. The distances between the inorganic layers, as indicated in Fig. S2, were measured over the converged crystals: for PEA_2PbI_4, d= 16.1 Å; for F-PEA_2PbI_4, d= 17.1 Å; and for MeO-PEA_2PbI_4, d= 17.5 Å; for $PEA_2MAPb_2I_7$, d= 16.1 Å; for F-$PEA_2MAPb_2I_7$, d= 16.6 Å; and for MeO-$PEA_2MAPb_2I_7$, d= 17.3 Å. These distances were close indeed to the experimental values reported in Fig. 1 of the main text.

Results

The chemical composition of 2D PVKs consist of the BOC bind to the metal halide, whereas for quasi 2D PVKs and 3D PVKs structures it is also necessary a small organic cation. Considering that through BOCs, it is possible to enrich the chemistry of the final materials by an adequate functionalization with the corresponding atom or functional groups on a pristine backbone, generating different interesting behaviors,[39] in addition, to the principal role that the organic moiety plays in the fabrication of high-quality thin films, we prepared and studied a set of 2D and quasi-2D PVKs, with nominal <*n*> =1 and 2, using three different cations with well differentiated electronic and structural properties, Scheme 1. The chosen cations are 1) phenylethylammonium (PEA), which is a cation widely studied and, therefore, with well-known properties.[29] Besides, the absence of any substituents on the aromatic ring makes it a perfect reference material; 2) 4-fluorophenylethylammonium (F-PEA), an ammonium cation substituted with a strong electronegative group as fluorine. Furthermore, it is known that this cation displayed interesting properties in the crystal lattice owing to the cation-cation interactions promoted by the fluorine substituent;[40-43] 3) 4-methoxyphenylethylammonium (MeO-PEA), with the presence of an electron-donating group. Consequently, we complete a set of cations including entirely all possible electronic features: electron-attracting, neutral and electron-donating groups. In addition, the presence of the bulkier MeO- group can have a potential effect not only on electronic but also crystallographic properties induced by both the size (steric hindrance) and the electron-donor properties (coordinative effect) of the methoxy group. [44-45]

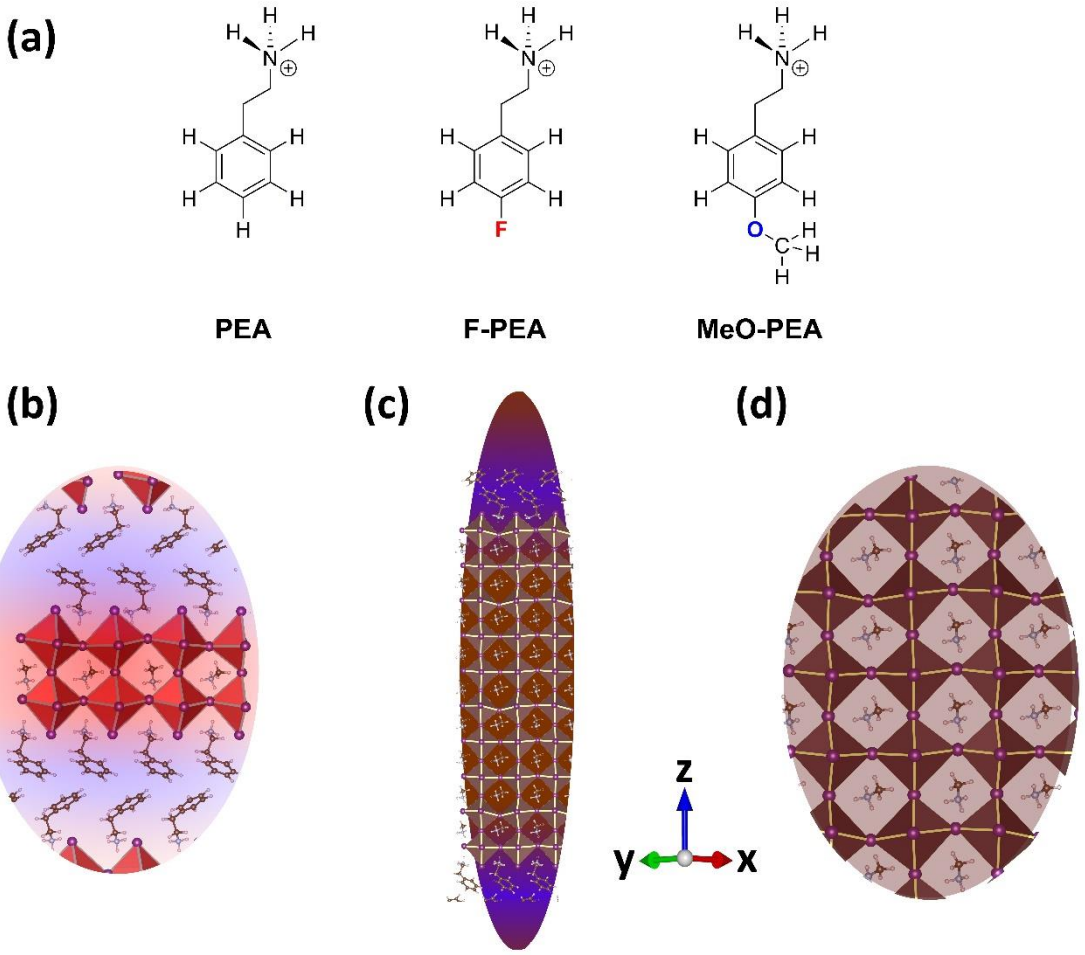

Scheme 1. (a) BOC used for fabrication of 2D PVKs investigated in the work. (b) 2D PVK with n=2. (c) Quasi 2D PVK with n=10. (d) 3D PVK. The blue shaded zone highlights different band gap value generating the quantum confinement effect observed in 2D materials. In contrast, the 3D PVK structure exhibit a single value of band gap.

As first step, we fabricate 2D/quasi-2D PVK thin films through the modified hot-casting process.[16] Posteriorly, we corroborated the formation of 2D phases through powder X-ray diffraction (*p*XRD) measurements (see Figure 1 a). For the materials with <*n*>=1 PEA_2PbI_4, F-PEA_2PbI_4 and MeO-PEA_2PbI_4, dominant diffraction peaks are found at 5.46º, 5.4º and 4.96º, respectively. The displacement to lower angles, ongoing from PEA_2PbI_4, to F-PEA_2PbI_4 and finally to MeO-PEA_2PbI_4, can be

assigned to the different size of the cations. Since PEA and F-PEA cations have similar sizes, it seems reasonable that we detect only a small shift of 0.08º for diffraction peaks. On the other hand, we can observe a remarkable shift of 0.52º in case of MeO-PEA owing to its bigger size in comparison to the previous ones. From *p*XRD patterns and Bragg´s law,[46] we calculate the interlayer distances, which are 16.1 Å, 16.4 Å, and 17.8 Å for PEA_2PbI_4, F-PEA_2PbI_4 and MeO-PEA_2PbI_4, respectively.

Assuming that the increase in the interlayer distances should be in a quantitative agreement with the increment of size for the series of the cations, the size of the cations was calculated; the found values are 6.74 Å, 6.88 Å and 8.43 Å, for PEA, F-PEA and MeO-PEA, respectively (See SI section 2.1, Figure S1). In addition, interplanar distance Pb-Pb was calculated by computational methods, resulting in very close distances to those calculated by experimental methods (see SI section 2.2, Figure S2). The cation size calculations show F-PEA and MeO-PEA are 2.1% and 25.1% larger than PEA, respectively (therefore, a calculated interlayer distance based on cations´ size should show similar values). Considering these values, the interlayer distances were compared in order to identify an effect into crystallization process due to the differences in size of each cation contrasting the experimental (pXRD values), theoretically (DFT calculations) and expected (assuming a linear packing of the BOC into the crystal lattice) well width.

The increase in the interlayer distance ongoing from PEA_2PbI_4 to F-PEA_2PbI_4 is 1.8%, while the expected increment, based on the increase of the cation size, should be 1.2%, see Figure 1b. We hypothesize that this slightly higher experimentally

measured increment of the interlayer distance as compared to that expected as function of the cation size can be due to a change in the crystal packing pattern in F-PEA_2PbI_4 as compared to PEA_2PbI_4; as a result of dissimilarity of the intermolecular interactions. The last, can be due to a change in the crystal packing pattern in F-PEA_2PbI_4 as compared to PEA_2PbI_4. When MeO-PEA is used as BOC, the expected interlayer distance (based on the cations sizes) should be 15.6% larger than that for PEA. However, this predicted increment results just in 10.6% based on *p*XRD measurements, see Figure 1b. This discrepancy between the expected and the experimentally measured interlayer distances suggests a variance in crystal packing, where MeO-PEA has a more advantageously packing than that observed in the case of F-PEA_2PbI_4, despite the potential stronger steric hindrance, promoted by the bulky nature of the CH_3-O-.

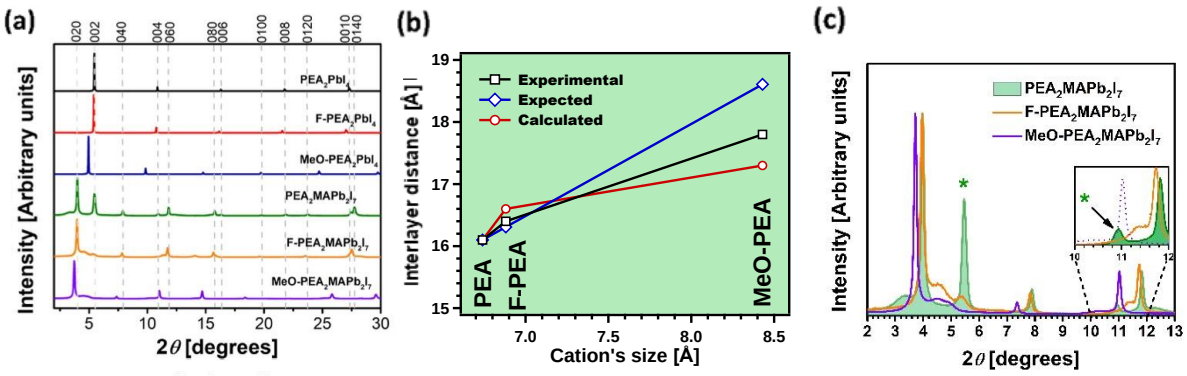

Figure 1. Morphological characterization by pXRD. a). X-ray diffraction patterns of (quasi)-2D perovskites with <n>=1, b) Interlayer distances obtained from experimental pXRD, estimated from BOC/PEA ratio, and calculated by DFT c) X-ray diffraction patterns of <n>=2 within the range from 2-13 degrees. For clarity, the solid line was substituted by a dashed line for MeO-PEA in the inset.

Concerning the preparation and characterization of $PEA_2MAPb_2I_7$, F-$PEA_2MAPb_2I_7$, MeO-$PEA_2MAPb_2I_7$ based thin films with <*n*>=2, the identification of differences in

the crystallization properties of the three materials, was possible, Figure 1a. The $PEA_2MAPb_2I_7$ *p*XRD diffractogram exhibits a diffraction peak at 3.98° which indicates the presence of n=2 phase as a principal component. Nevertheless, it is possible to detect a considerable concentration of n=1 phase, observed at 5.46º, 10.94º, etc., see Figure 1c. In addition, a more carefully analysis enables one to detect a shoulder at 3.28°, which could be ascribed to n=3 phase, Figure 1c.[27] Surprisingly, when F-PEA or MeO-PEA are used, a dominant diffraction peaks is detected at 3.96º and 3.72º, respectively, related to n=2 phase, although a minimal concentration of n=1 phase seems to be present for the F-PEA based material and, additionally, it is possible to detect a shoulder between n=1 and n=2 diffraction peaks. Regarding MeO-$PEA_2MAPb_2I_7$, the *p*XRD pattern did not exhibit any peaks associated with n=1 or n>2 phases, as observed in case of PEA films, although the earlier mentioned shoulder in F-$PEA_2MAPb_2I_7$ film is still visible here, but with lower intensity.

In the absorbance spectra for the materials with <*n*>=1 (Figure S3) we observe the exciton resonances centered at 516 nm (2.403 eV), 513 nm (2.417 eV) and 514 nm (2.412 eV) for PEA_2PbI_4, F-PEA_2PbI_4 and MeO-PEA_2PbI_4, respectively. We cannot extract accurately their corresponding bandgap energies, because the exciton continuum offset is not clearly observed, which is attributed to the inhomogeneous broadening associated to these polycrystalline films, as previously reported.[47] However, in the case of the films with <*n*>=2 we can observe slight differences in the absorption spectra of the films of the different BOCs (Figures 2a and c), specially at 20K (Figure 2c), where we can observe the 2s exciton resonance for the n=1 (strictly 2D PVK) and even for n=2 in the case of PEA (see arrows in Figure 2c). In

fact, the energy difference between 1s and 2s exciton resonances would be approximately 333, 263 and 246 meV for PEA_2PbI_4, F-PEA_2PbI_4 and MeO-PEA_2PbI_4, respectively. This observed reduction in energy from PEA to MeO-PEA could be related to a certain cutback of the exciton binding energy promoted by the introduction of the respective moiety that potentially could more efficiently screens the carriers.[14] It is also interesting to note the observed reduction in the 1s-2s energy difference to ≈ 140 meV for the film of PEA with <*n*>=2 (green curve in Figure 2c), which is consistent with the expected decrease in the exciton binding energy by increasing n (thicker QWs with quasi-2D confinement).[48] Relaying on its behavior, the optical properties for <*n*>=2 thin films are summarized as follows: 1) the one typically observed, where the prepared films exhibit the presence of a distribution of QWs with different number of octahedral layers (n=1,2,3…), despite the stoichiometric relationship established in the chemical formulation of the precursors. Considering that the target films are those with two octahedra monolayers, i.e. <*n*>=2, the recorded spectra were normalized using n=2 absorption/PL peaks as reference to compare the signal ratio of the different phases in all samples. The classical behavior was observed for $PEA_2MAPb_2I_7$ thin films where, at 300K (green curves in Figures 2a-b), it was possible to detect at least three resonances at 517, 568 and 608 nm (in absorption, Figure 2a), which can be assigned to n= 1, 2 and 3 excitonic transitions, respectively, in agreement with literature,[21] and with our *p*XRD results described above. 2) the non-typical observation, where the fabricated films do not show absorbance peaks for high *n*-phases, even reaching the 3D limit. In contrast with the first behavior, in this one it seems that the obtained thin films follow

the stoichiometric relationships established in the formulation, obtaining a reduced quantum wells thickness polydispersity. This behavior was observed in the case of F-$PEA_2MAPb_2I_7$ and MeO-$PEA_2MAPb_2I_7$, as corroborated by *p*XRD and absorbance spectroscopy (orange and purple curves in Figure 2a). Both BOC-based thin films present clear electronic transitions corresponding to n=1 and 2 phases, namely at 518 and 568 nm, although a shoulder associated to the n=3 phase can be detected in their corresponding spectra, but weaker than in the case of the reference PEA based quasi-2D PVK based thin-film.

Concerning PL (Figure 2b), $PEA_2MAPb_2I_7$ thin films exhibit PL lines centered at 523, 579 and 625 nm, again attributed to n= 1, 2 and 3 phases, respectively, plus a wide and pronounced emission band centered at 754 nm, which would be consistent with the existence of a wide distribution of QW thicknesses or higher *n* phases and even the limit of the 3D $MAPbI_3$ perovskite. This observation is also associated to a very efficient charge carrier funneling from the higher (low-*n*) to lower (high-*n*) energy band gap phases.[49] It is important to highlight that, while the relative intensities observed for the PL bands of $PEA_2MAPb_2I_7$ suggest a relatively important concentration of such high-*n* phases (+3D PVKs), the PL spectra of F-$PEA_2MAPb_2I_7$ and MeO-$PEA_2MAPb_2I_7$ thin films indicate a negligible contribution of these phases and the dominant presence of the target *n*=2 phase, as shown Figure 2b.

The absorbance spectra at 20K of quasi-2D PVKs thin films (Figure 2c) are very similar to those described above at 300K but giving clearer evidence of our hypothesis. In fact, the absorbance spectrum $PEA_2MAPb_2I_7$ (green curve) exhibits clearer excitonic bands related to n= 1, 2, 3 and even 4. Additionally, it is possible to

observe that the excitonic transition related to n=1 phase demonstrates an absorption strength comparable to that of the n=2 phase. In contrast, the absorbance spectra at 20K for the films prepared with F-$PEA_2MAPb_2I_7$ and MeO-$PEA_2MAPb_2I_7$ (orange and purple curves) show only two dominant excitonic transitions, for n=1 and 2, being the latter the dominant. Indeed, the excitonic transition corresponding to n= 3 phase for these two materials show a considerably reduced intensity of only a 10% of the n=2 phase, as compared to the 25 % in the case of $PEA_2MAPb_2I_7$.

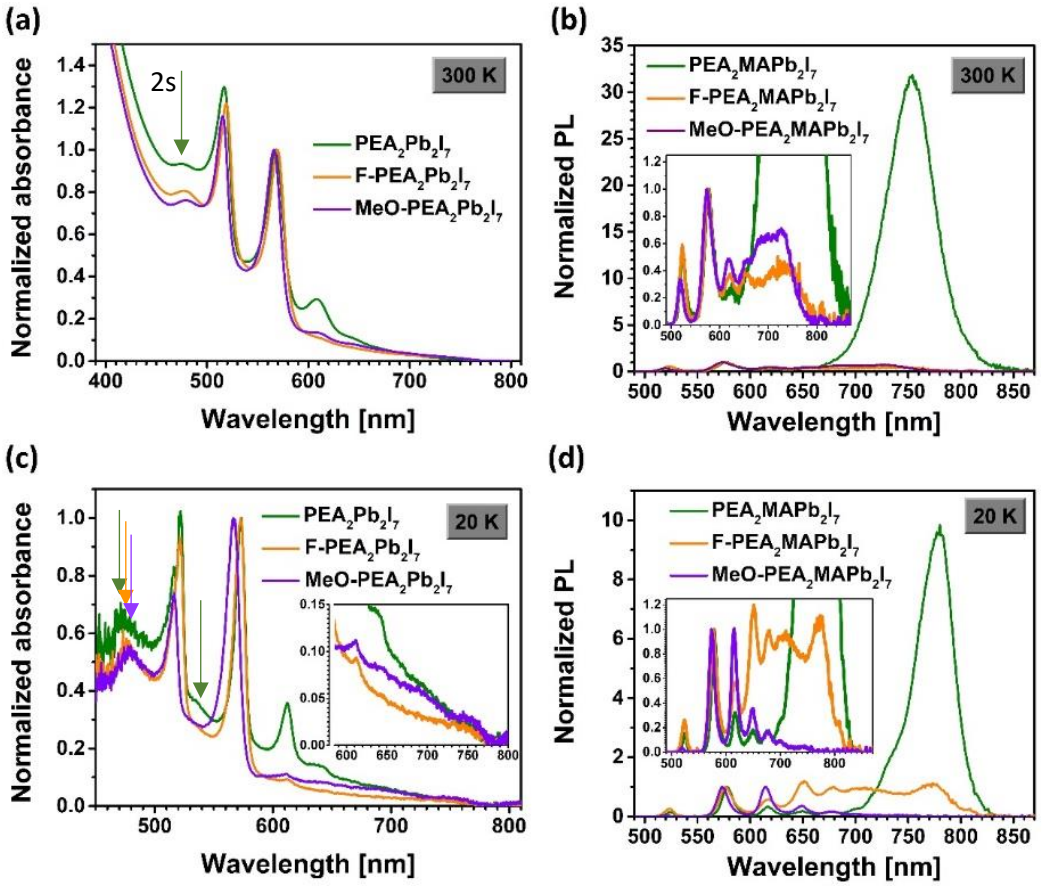

Figure 2. Optical characterization at 300K and 20K for $PEA_2Pb_2I_7$, F-$PEA_2Pb_2I_7$ and MeO-$PEA_2Pb_2I_7$ based thin films. Absorption measurements excitation was realized by 100 fs pulses at 405 nm with a fluence between 0.2 and 2.4 nJ/cm^2 per pulse.

In agreement with the results observed in absorption spectroscopy, the PL spectrum at 20K for $PEA_2MAPb_2I_7$ (green curve in Figure 2d), corroborates the important QW distribution with random sizes $1 < n < \infty$ (see clear PL lines from n = 1 to n =5), and mostly the contribution of the 3D perovskite, pressing an intensity significantly higher than the rest of the peaks. In contrast, the PL of F-$PEA_2MAPb_2I_7$ and MeO-$PEA_2MAPb_2I_7$ thin films (orange and purple curves in Figure 2d) that also exhibits the contributions from n = 1 to n =5 phases and the 3D at 780 nm, but the intensity of 3D PVK is comparable with the intensities produced by the different n orders. It is worth to stress their contribution as compared to the reference material $PEA_2MAPb_2I_7$, being negligible the fingerprint of the 3D phase in the case of MeO-$PEA_2MAPb_2I_7$.

In above-described experiments we excited the samples with a low-intensity pulse excitation laser source (excitation at 405 nm with fluence between 0.2 and 2.4 nJ/cm_2). Such low-intensity excitation models are similar to the conditions observed in photovoltaic and optoelectronic devices. However, it is necessary to consider that, under such low-intensity excitation conditions, the relative intensities of the PL bands corresponding to low-*n* phases are not proportional to the physical concentrations of these phases, because of the very fast funneling of excited carriers from low- to higher-*n* phases.[49-50] The funneling is a sort of quenching process from the point of view of lower-n phases, which decreases intensity of the corresponding bands in steady-state PL spectra. Based on these considerations, we conclude that if we excite our samples with powerful light pulses, thus increasing the instantaneous concentration of carriers, this should lead to an increase in the radiation

recombination rate constant, which is proportional to the square of the carrier concentration. In this case, radiation can become the dominant process of deactivation of excitons for low-n phases, while excitation funneling will be in this case a minor process. We expect that the increase in the intensity of the low-*n* PL bands with increasing excitation intensity will be especially significant at 20K, when the processes of nonradiative deactivation of excitons, which compete with both radiative recombination and funneling, are deactivated. The obtained results are showed in the Figure 3, for details of the experiment see SI. The PL spectrum measured under high excitation fluence regime for $PEA_2MAPb_2I_7$ (green curves in Figure 3) demonstrates a dominant strong emission band centered at ~744 nm originated from higher *n* phases and probably a certain contribution of the 3D perovskite. Besides, it was possible to detect a similar behavior at 20K (Figure 3b), where, again, clear excitonic peaks are observed for phases n=1, 2, 3, 4 and 5 and even the broad band peaked at around 775 nm, which exhibits shoulders that could correspond to phases with n=6-9. Regarding F-$PEA_2MAPb_2I_7$, the PL spectrum at 300K exhibit the peak associated to n=2 as the dominant transition, with a little contribution of the n= 1 phase (lower than 10%), as observed in Figure 3a; moreover, it is possible to see the presence of a broad band from ~ 620 to 800 nm, which can be resolved at 20K (orange curve in Figure 3b) revealing the presence of excitonic peaks for n = 3 - 5 and the broad band centered at 772 nm. Although at both 300K and 20K it was possible to detect higher phases and 3D perovskite, their smaller intensity as compared to the $PEA_2MAPb_2I_7$ thin film suggests that the inclusion of the F-PEA cation effectively reduces the quantum well polydispersity, in agreement with the results described above.

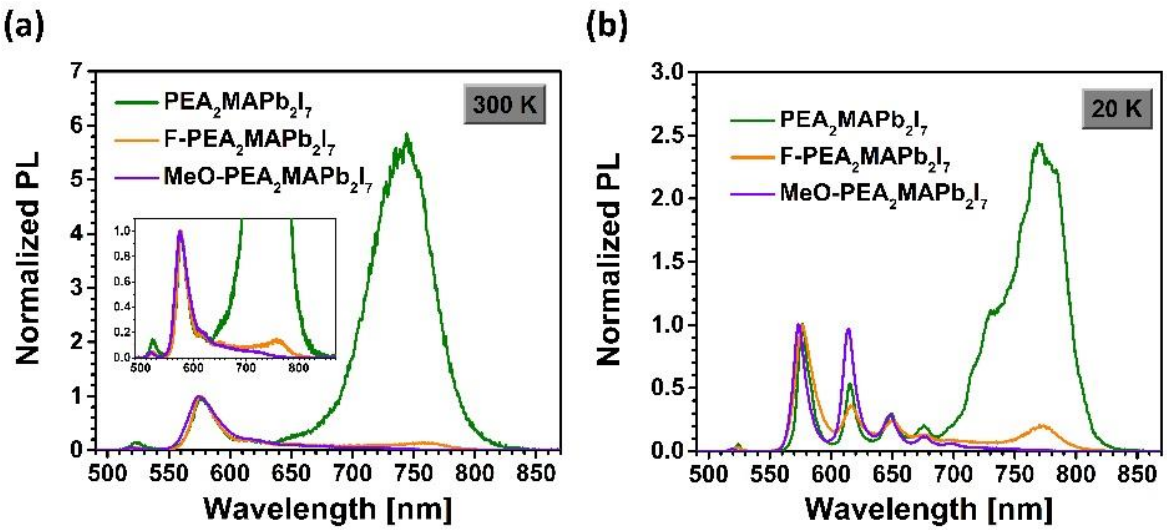

Figure 3. Optical characterization at 300K and 20K for $PEA_2Pb_2I_7$, F-$PEA_2Pb_2I_7$ and MeO-$PEA_2Pb_2I_7$ based thin films at higher fluence intensities. Excitation was realized by 100 fs pulses at 405 nm with fluence between 200 nJ/cm^2 and 17 µJ/cm^2 per pulse.

Finally, the spectra of MeO-$PEA_2MAPb_2I_7$ (purple curves in Figure 3) depict similar tendency about the control of the QW polydispersity. The PL spectrum at 300K (Figure 3a) exhibit a dominant peak for n=2 phase and a considerably weaker broad band from ~620 to 720 nm. Again, at 20K was possible to resolve this broad band into different and weak excitonic peaks that are associated to phases with n= 3, 4, 5 and 6, without traces of PL beyond 720 nm. Therefore, it is very clear the beneficial influence of the use of fluorine or methoxy as substituents of the BOC cations in order to obtain an effective reduction of the QW polydispersity as compared to the reference BOC without any substitution, as PEA. In other words, the formation of higher-*n* phases and QW polydispersity were certainly controlled by using substituted BOCs.

In conventional 3D perovskites, it is known that the organics, i.e., ammonium salts, perform a key role as coordinating agent to stabilize/solubilize the inorganic moiety in the precursor colloidal suspension and the coordination complex is responsible of the quality of the acquired thin films.[33] Concerning 2D PVKs, there are consistent evidences of the preparation of single-phase materials with n>1, however these successful methods are principally restricted to single crystals.[9, 27-28] Recently, Liang et. al reported the fabrication of single-phase 2D perovskites thin films. The authors hypothesize that the strong control of the well width was achieved through an increase in the bonding interactions of butylammonium acetate and the perovskite framework in the precursor solution, -specifically between the evaluated acetate counterion instead of the widely used iodide-.[32] In that work, the addition of acetate as counterion, a stronger Lewis base than iodide anion, produce the size reduction of colloidal particles in the precursor solution to sizes as small as 1 nm (in a first statement they establish the dominant interaction is between acetate anion and Pb^{2+} ion). Their results suggest that it is possible to reduce, or even suppress, the formation of undesired different *n* phases (not only those near to the 3D limit) by the introduction of a strong coordinating agent. It seems that this slight change could limit the formation of aggregates with different sizes, and therefore different numbers of stacked $[PbI_6]^{4-}$ sheets, favoring the observation of a reduced number of *n* phases. It is possible to reach similar conclusion, although from a contrasting point of view, through the work by Kong et. Al. They demonstrated that during the fabrication of quasi-2D perovskites, the inclusion into the formulation of a robust anion as methansulfonate, with a powerful basic character, leads to the observation of a strong hydrogen bonding interaction between methansulfonate and the BOC salt.

This fact limits the coordinating ability of the BOC towards $[PbI_6]^{4-}$ octahedra, inducing the preferent observation of large *n* phases, even 3D perovskite, instead small *n* phases.[51] Therefore, these studies suggest that the different interaction that experiments $[Pb^{2+}]$ or $[PbI_6]^{4-}$ octahedra for determined species in the coordination sphere, could determines not only the quality of the fabricated thin films, but also the *n*-phases observed in the synthesized 2D PVKs materials. Due to these results, colloidal suspensions of the prepared 2D PVKs were prepared and analyzed by dynamic light scattering (DLS) with the aim to detect a possible relation between the cations and differences in population distribution. The samples studied correspond to quasi-2D PVKs precursor solutions with a $<n>=2$, using the three different BOCs. The set of diffractograms exhibit two size distributions, one of them in the range of 30-70 nm and the second one between 0.3 and 4 μm, Figure 4a. The observation of two populations could be related to the different coordination properties of the solvents used in the preparation of solutions (DMSO and DMF).[32, 52] On one hand, DMSO/perovskite precursors interactions are characterized by a relatively strong Pb-O bound with a Gutmann´s donor number (D_N) of 29.8 Kcal mol^{-1} and 2.386 Å of bond length.[53-55] Such bounds promote the formation of $[PbI_6]^{4-}$ complexes,[56] which will lead to the growing of small colloidal nanoparticles. On the other hand, DMF/perovskite precursors have weaker Pb-O bounds (2.431 Å of bond length and D_N of 26.6 Kcal mol^{-1}) which allow more interactions between DMF, $CH_3NH_3^+$ and Pb^{2+} that promote the formation of several lead coordination species, resulting in the agglomeration of particles out of the range of colloidal size.[52, 56-57] In our particular situation, considering that the obtained results suggest that each of the substituents on the aromatic ring of the BOC introduce different properties, as for example

coordination bonding characteristic in the precursor solutions, each of them must play an important role in the formation of the lead complexes, hence in the size of the precursor suspended particles. To monitor the effect of the substituents in the proportion between small colloidal particles and big particles agglomerates the DLS peaks intensities ratio was analyzed in Figure 4b. However, even when the precursor solutions behave in a similar way concerning to the number of populations and peak intensities, their relative concentrations, is contrasting. It was observed that when PEA BOC is used, the colloidal nanoparticle peak is centered at 63 nm (peak 1) and the peak corresponding to particle agglomerates (peak 2) is centered at 1310 nm with a peak 1/peak 2 intensity ratio of 0.74, *i.e*., the concentration of colloidal nanoparticles is ~25% lower than particle agglomerates. The dominance of peak 2 over peak 1, suggest that the use of PEA as BOC promotes the formation of big agglomerates over the formation of colloidal nanoparticles. In contrast, the diffractograms for F-$PEA_2MAPb_2I_7$ and MeO-$PEA_2MAPb_2I_7$ based materials show that the concentration of colloidal nanoparticles is 3% and 31% higher than agglomerates, respectively. When the substituted cations are used, two mean effects are observed. 1) The signal corresponding to small particles shifts to smaller sizes, to 49 nm and 50 nm, for F-PEA and MeO-PEA, respectively, and 2) the nanoparticle/agglomerate signal ratio is increased beyond 1, indicating that the use of any of these cations not only promotes the formation of smaller nanoparticles but also limits de formation of particle agglomerates, favoring the obtention of dispersed colloids of nanoparticles, which help us to obtain a reduced phase polydispersity.

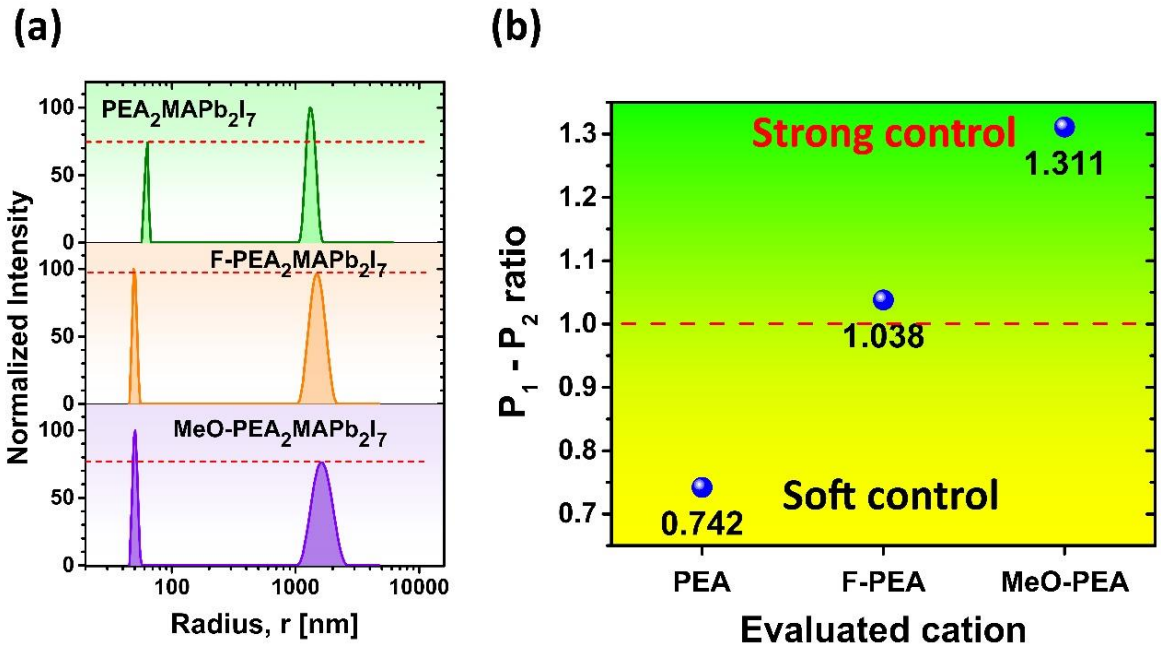

Figure 4. (a) Size populations obtained by DLS from $PEA_2MAPb_2I_7$; F-$PEA_2MAPb_2I_7$; MeO-$PEA_2MAPb_2I_7$. Two populations are recorded. The red line shows the relation between the lower occupied population comparing to the dominant population. (b) Ratio between the corresponding size populations. When the P_1-P_2 ratio < 1, the control of *n*-phases is soft or even inexistent. In contrast when P_1-P_2 > 1, the control becomes stronger and the quantum well polydispersity is controlled.

Therefore, we can conclude that the control observed in the reduction of *n*-phase polydispersity in our materials could be related not only to the reduction in the particle size[32], but also to the ratio between the observed population, which is a consequence of the different properties of the BOCs used to prepare the precursor solution of each material.

According to the literature, a small size distribution could be related with no aggregation of colloids, promoting therefore the formation of desired small *n* phases. In contrast, a big size distribution seems to be associated with a high degree of colloids aggregation, favoring the formation of high *n* phases near to the 3D limit.[32]

Additionally, the interaction between the BOC and another molecule allows a free inorganic nanosheet formation, and their stacking growth, increasing the proportion of large-*n* phases in the overall perovskite film.[51] This suggest that the application of a BOC with an stronger bonding interaction between them and the inorganic sheet, will lead to reach better control about *n* phase polydispersity, as previous results suggested.

To corroborate this hypothesis, we perform NMR experiments with the aim to evaluate a potential relationship between a reduced polydispersity and a stronger interaction in the liquid state between BOC and the inorganic semiconductor sheets. First, we prepare a set of the precursor solutions of the studied materials. Figures S4a-c shows the spectra for these cations separately, as well as a comparison between them (Figure S4d). The NMR spectra show a constant shift to lower frequencies for the signals originated from the hydrogens on ammonium head on going from PEA (7.77 ppm) to F-PEA (7.75 ppm) and MeO-PEA (7.72 ppm), which implies that those hydrogens become less acid due to the intrinsic nature of each molecule. When PbI_2 + MAI is added at the corresponding solutions, it is observed an additional shift to lower frequencies for all the materials (7.60, 7.60 and 7.58 ppm for PEA, F-PEA and MeO-PEA, respectively), Figure 5 and Figure S4e, which could be owing to the N-H ··· I hydrogen bonding interaction, *protecting* the referred hydrogens on each of the studied BOCs, Figure 5.[58] Although, the hydrogen bonding has and important effect on control of n-phase segregation through the colloidal size modulation, F-PEA have other effects such as strong π-π interactions that should not be underestimated, because the van der Waals interactions promotes the

parallel arrangement of the phenyl groups.[38, 59] This interaction among phenyl rings might cause steric hindrance as beneficial side effect because it could limit the non-covalent interactions with other constituents of the precursor solution, i.e., interactions with solvents and MAI. In this sense limiting the sizes of particles of the solution, driving the preferential colloidal size particles formation instead of out-of-range colloidal size particles. The observation through ^{1}H NMR of a stronger hydrogen bonding interaction for F-PEA and MeO-PEA than PEA based materials agree with our hypothesis where the modification of coordinative properties, is the responsible to the better control to reduce the *n*-phase polydispersity through the limitation of microscopical agglomerates. This finding supports the fact described by Liang,[32] where a strong interaction between $[PbI_6]^{4-}$ and other species, in our case the BOCs in their case an extra molecule, avoid the formation of not only large agglomerates but also reduced number of populations.

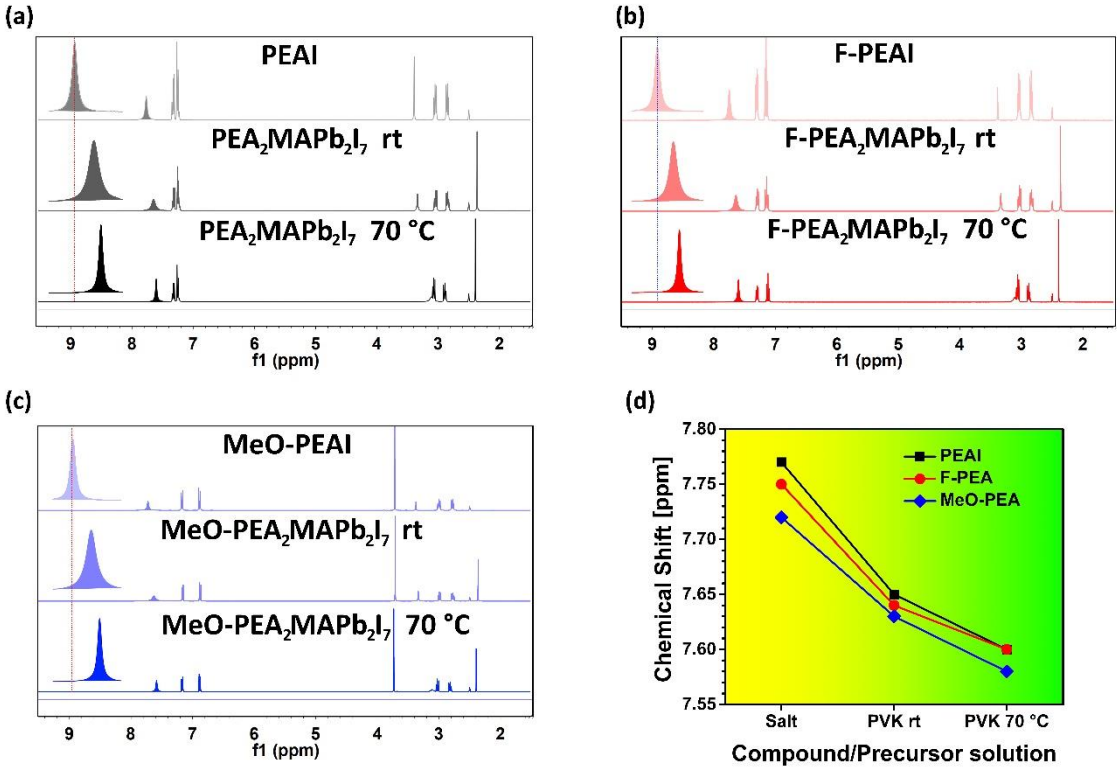

Figure 5. ^{1}H NMR spectra for 2D PVKs, DMSO-d6; 400 MHz. (a) ^{1}H NMR for PEA based systems; (b) ^{1}H NMR for F-PEA based systems; (c) ^{1}H NMR for MeO-PEA based systems. (d) Chemical shift for the N*H*$_3$ resonances for the salts and the PVKs precursor solution at rt and high temperature. The shaded highlighted peaks in a-c correspond to the H-N signals on each of the spectra located near 8 ppm.

As the hot-casting process that we used in the fabrication of thin films requires the heating of the precursor solutions, we also evaluate ^{1}H NMR spectra at 70 °C, Figure 5a-c bottom. Interestingly, all samples show additional shift to lower frequencies when NMR spectra are acquired at higher temperatures, which suggest the hydrogen bonding interaction between all the BOCs and the $[PbI_6]^{4-}$ octahedra not only remains, but also becomes stronger than those observed at room temperature. The comparison of the three precursor solutions shows that F-PEA and MeO-PEA cations exhibit, one more time, stronger hydrogen bonding interaction than PEA.

Again, this observation agrees with the hypothesis, where a stronger interaction between the BOC and the inorganic sheets, induces a better *n*-phase polydispersity control. The ^{1}H NMR spectra at 70 °C for the bulky cations showed a very little shift compared with those acquired at room temperature (~ 0.03 ppm) (Figure S5). This observation supports the hypothesis that the strong shift observed in the ^{1}H NMR spectra (0.17, 0.15 and 0.14 ppm for PEA, F-PEA and MeO-PEA, respectively) of the perovskite precursor solution can be related to the bonding interaction between the organic and inorganic species.

To corroborate the intermolecular bonding interaction properties of the BOCs are the main responsible of the suppression of the 3D PVK phase, we prepare two additional batches of samples. The first one includes PEA cation, which shows a lower bonding interaction, and the second formulation excluding it. Therefore, the former formulation has the formula ((PEA/MeO-PEA)$_2$MAPb$_2$I$_7$) and the second one is ((F-PEA/MeO-PEA)$_2$MAPb$_2$I$_7$). If the hypothesis is correct, the formulation including PEA as BOC must promote the observation of n>>2 or even 3D PVK phase; while that in the formulation based on stronger coordinating BOCs, must be observed a reduction on the quantum well polydispersity, and therefore the observation of <*n*>=2 must be the dominant. For (PEA/MeO-PEA)$_2$MAPb$_2$I$_7$, the *p*XRD pattern (Figure 6a) shows not only the n=2 related peak, at 3.88°, but also the diffraction peaks originated for n=1 and n=3 phases at 5.22° and 2.92°, respectively. In a similar way, absorbance spectrum (green-shadowed curve in Figure 6b) shows a well-defined exciton resonance at 560 nm confirming the presence of the n= 2 phase but accompanied of a very strong resonance at 520 nm indicating a very significative amount of the

n=1 phase, and the presence of weaker contributions at λ > 600 nm, evidencing small amounts of n = 3 and n=4 phases. The corresponding PL spectrum (green-shadowed curve in Figure 6c) also shows three well defined peaks between 500 to 650 nm confirming the findings in absorbance, but it also shows a broad band between 650 and 750 nm indicating the presence of n≫2 phases. Contrarily, (F-PEA/MeO-PEA)$_2$MAPb$_2$I$_7$ *p*XRD diffractogram shows a dominant peak at 3.86° which correspond to n=2 phase. The shift to lower angles agrees with the behavior exhibited by the material studied in the past section, where the higher size of the used cation, specifically the large size of MeO-PEA, increase the interlayer distance of the inorganic semiconductor. In contrast to the previous material, the absorbance spectrum for the (F-PEA/MeO-PEA)$_2$MAPb$_2$I$_7$ films (pink-shaded curve in Figure 6b) exhibit the resonance related to the n=2 phase as the main contribution, with the lowest contribution of n=1 and 3 phases, even comparing to pure F-PEA$_2$MAPb$_2$I$_7$ and MeO-PEA$_2$MAPb$_2$I$_7$ materials. Besides, its PL spectrum (pink-shaded curve in Figure 6c) indicates that (F-PEA/MeO-PEA)$_2$MAPb$_2$I$_7$ samples not only have the lowest contribution of the n=1 and n= 3 phases, but also that the formation of higher phases and quantum wells polydispersity were certainly absent/reduced.

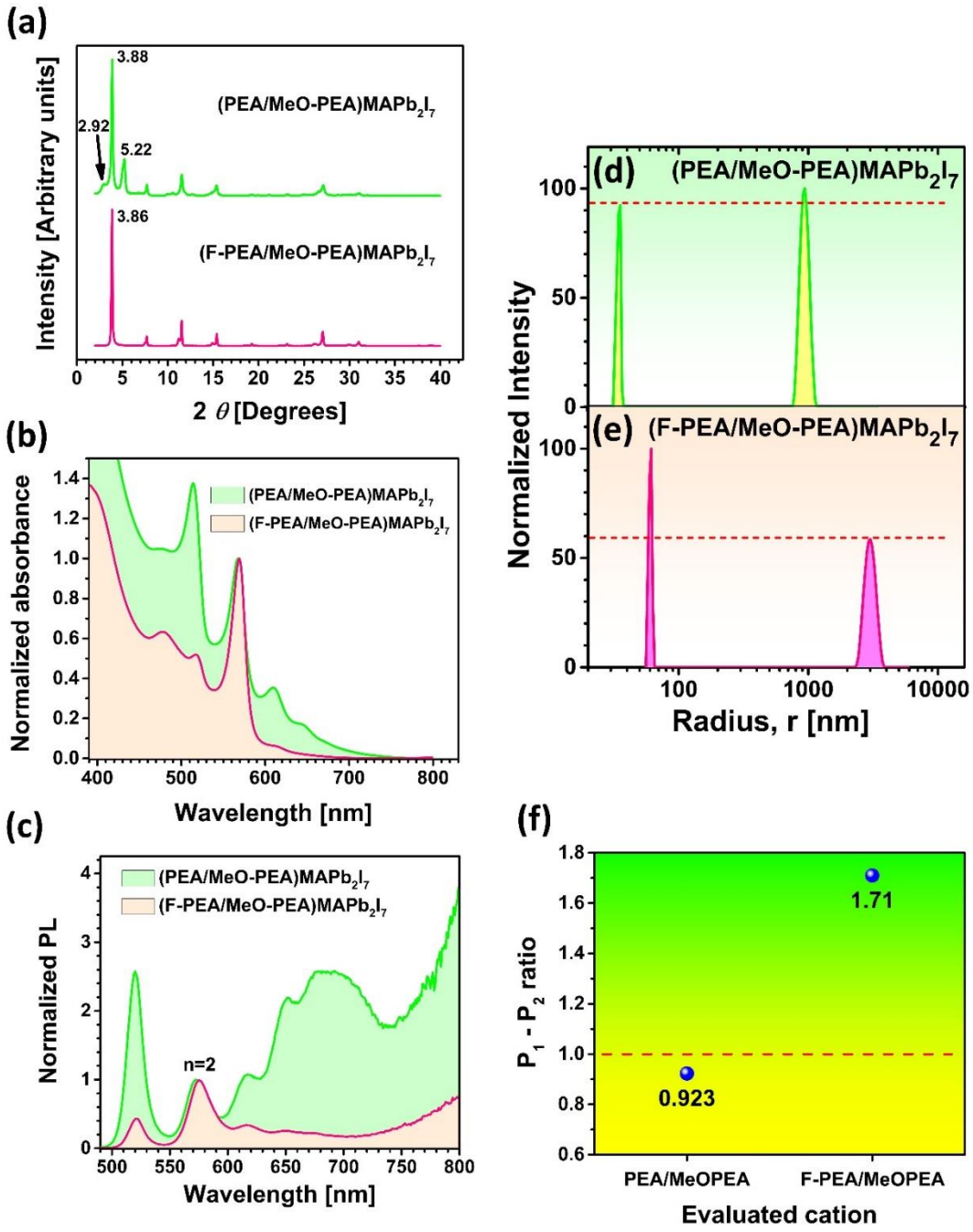

Figure 6. Characterization for 2D PVK with <*n*>=2 using a 1:1 mixture of BOCs: (PEA/MeO-PEA)$MAPb_2I_7$ (green) and F-PEA/MeO-PEA)$MAPb_2I_7$ (pink). (a) *p*XRD; (b) absorbance spectroscopy; (c) PL spectroscopy; (d) and (e) DLS diffractograms; (f) P_1/P_2 ratio. The sample containing the F-PEA and MeO-PEA cations exhibit an improved control about n-phase polydispersity, related to their better bonding interaction properties. In contrast, the precursor solution prepared with the PEA cation leads to get a wide n-phase polydispersity.

Concerning the DLS results, it was possible to detect a slightly dominant formation of agglomerates over colloids for $(PEA/MeO\text{-}PEA)_2MAPb_2I_7$, Figure 6d and f, where the ratio between both populations is practically 1:1. However, it is important to highlight that the MeO-PEA cation has a positive effect when it is introduced in the formulation, considering the important increase in the colloids concentration compared to the observed in $PEA_2MAPb_2I_7$, Figure 4, where the concentration of agglomerates is the dominant. In contrast, unlike PEA-formulation, it can be observed that when F-PEA or MeO-PEA are used as BOCs, the formation of colloids is strongly favored over the microscopical agglomerates, as the concentration of the formers is 71% higher than the observed for microscopical agglomerates, Figure 6e, and f, the best of the samples studied in this work.

The facts observed in this work, together the observations of the literature,[32-34] suggest there are some features related to the "medium" (can be very coordinating solvent, anions, or, as in this particular case, cations) around the inorganic species can promote or inhibit the observation of determined phase. In this work we could observe that, a light modification (different substituent: H Vs F Vs MeO) in a common backbone (the phenyl ring) lead to the dominant observation of 3D PVK phase (H-substituted) or a <n>=2 phase (MeO- substituted). Based on the results, we hypothesize the inclusion of very bulky cations, highly spatially hindered, and that shows a very effective bonding interaction with the inorganic species will promote the observation of 2D phase. In contrast, the application of cations (can be very similar between them, like in this work) that allows, or even promote, the interaction between the inorganics, will lead to the observation of higher or even 3D perovskite phases.

CONCLUSIONS

We have demonstrated that the use PEA, F-PEA and MeO-PEA cations allows the fabrication of 2D PVKs based thin films with very different *n*-phase polydispersity. By *p*XRD, absorbance and PL characterization, it was possible to determine that the used BOCs follows the order MeO-PEA>F-PEA>PEA to control the n-phase polydispersity and obtain the desired n=2 with higher phase purity. DLS results demonstrate that the number of observed populations, or ratio between them, as well as the size of the particles in the liquid state are in function of the cation. A stronger interaction between BOC and the inorganic moiety reduces the size of the particles in the precursor solutions, favoring the formation of particles in the colloidal size range. In the same way, the observation of colloidal nanoparticles generates the formation of the desired n=2 phase instead of higher *n*-phases or 3D PVKs. In contrast, the observation of large agglomerates promotes the formation of n>>2 or 3D PVKs phases. By ^{1}H NMR spectroscopy, it was possible to determine the presence of an effective bonding interaction between the corresponding BOC and the inorganic species in the precursor solution. The observed tendency follows the order MeO-PEA>F-PEA>PEA, where MeOPEA undergo the stronger intermolecular bonding interaction, in spite of the potential steric hindrance promoted by the MeO-group. Importantly, similar tendency was observed at high temperature (70 °C). We found that the fabrication of 2D perovskite with a reduced n-phase polydispersity, can be possible using cations with different interaction properties, where the use of extra reagents/additives it is no necessary.

Acknowledgments

This work was made possible by the Horizon 2020 research and innovation program through the DROP-IT project (grant agreement No. 862656), the Spanish MINECO through the project No. TEC2017-86102-C2-1-R, the ministry of Science and Innovation of Spain under Project STABLE PID2019-107314RB-I00, the European Research Council (ERC) via Consolidator Grant (724424 - No-LIMIT), the University Jaume I (Project DEPE2D UJI-B2019-09) and the PAIP-UNAM through the project No. 5000-9190. We are very grateful to Rosa Isela del Villar Morales and Nayeli Lopez Balbiaux for the acquisition of NMR spectra. R.V.-C. thanks the financial support from CONACYT under grant 445257.

Supporting information description

Cation´s and interlayer distances´ images. ^{1}H NMR spectra of cations and perovskite precursor solutions at room and higher temperatures.

References

1. Nakajima, T.; Yamauchi, H.; Goto, T.; Yoshizawa, M.; Suzuki, T.; Fujimura, T., Magnetic and elastic properties of (CH3NH3)2FeCl4 and (C2H5NH3)2FeCl4. *J. Magn. Magn. Mater.* **1983,** *31-34*, 1189-1190.

2. Ishihara, T.; Takahashi, J.; Goto, T., Exciton state in two-dimensional perovskite semiconductor (C10H21NH3)2PbI4. *Solid State Commun.* **1989,** *69* (9), 933-936.

3. Calabrese, J.; Jones, N. L.; Harlow, R. L.; Herron, N.; Thorn, D. L.; Wang, Y., Preparation and characterization of layered lead halide compounds. *J. Am. Chem. Soc.* **1991,** *113* (6), 2328-2330.

4. Mitzi, D. B.; Feild, C. A.; Harrison, W. T. A.; Guloy, A. M., Conducting tin halides with a layered organic-based perovskite structure. *Nature* **1994,** *369* (6480), 467-469.

5. Kagan, C. R.; Mitzi, D. B.; Dimitrakopoulos, C. D., Organic-Inorganic Hybrid Materials as Semiconducting Channels in Thin-Film Field-Effect Transistors. *Science* **1999,** *286* (5441), 945-947.

6. Ishihara, T.; Takahashi, J.; Goto, T., Optical properties due to electronic transitions in two-dimensional semiconductors (CnH2n+1NH3)2PbI4. *Phys. Rev. B-Conden Matter* **1990,** *42* (17), 11099-11107.

7. Hong, X.; Ishihara, T.; Nurmikko, A. V., Dielectric confinement effect on excitons in PbI_4-based layered semiconductors. *Phys. Rev. B* **1992,** *45* (12), 6961-6964.

8. Tsai, H.; Nie, W.; Blancon, J.-C.; Stoumpos, C. C.; Soe, C. M. M.; Yoo, J.; Crochet, J.; Tretiak, S.; Even, J.; Sadhanala, A.; Azzellino, G.; Brenes, R.; Ajayan, P. M.; Bulović, V.; Stranks, S. D.; Friend, R. H.; Kanatzidis, M. G.; Mohite, A. D., Stable Light-Emitting Diodes Using Phase-Pure Ruddlesden–Popper Layered Perovskites. *Adv. Mater.* **2018**, *30*, 1704217-n/a.

9. Cao, D. H.; Stoumpos, C. C.; Farha, O. K.; Hupp, J. T.; Kanatzidis, M. G., 2D Homologous Perovskites as Light-Absorbing Materials for Solar Cell Applications. *J. Am. Chem. Soc.* **2015,** *137* (24), 7843-50.

10. Tsai, H.; Nie, W.; Blancon, J.-C.; Stoumpos, C. C.; Asadpour, R.; Harutyunyan, B.; Neukirch, A. J.; Verduzco, R.; Crochet, J. J.; Tretiak, S.; Pedesseau, L.; Even, J.; Alam, M. A.; Gupta, G.; Lou, J.; Ajayan, P. M.; Bedzyk, M. J.; Kanatzidis, M. G.; Mohite, A. D., High-efficiency two-dimensional Ruddlesden–Popper perovskite solar cells. *Nature* **2016,** *536*, 312.

11. Mao, L.; Wu, Y.; Stoumpos, C. C.; Traore, B.; Katan, C.; Even, J.; Wasielewski, M. R.; Kanatzidis, M. G., Tunable White-Light Emission in Single-Cation-Templated Three-Layered 2D Perovskites (CH3CH2NH3)4Pb3Br10-xClx. *J. Am. Chem. Soc.* **2017,** *139* (34), 11956-11963.

12. Straus, D. B.; Kagan, C. R., Electrons, Excitons, and Phonons in Two-Dimensional Hybrid Perovskites: Connecting Structural, Optical, and Electronic Properties. *J. Phys. Chem. Lett.* **2018,** *9* (6), 1434-1447.

13. Gelvez-Rueda, M. C.; Hutter, E. M.; Cao, D. H.; Renaud, N.; Stoumpos, C. C.; Hupp, J. T.; Savenije, T. J.; Kanatzidis, M. G.; Grozema, F. C., Interconversion between Free Charges and Bound Excitons in 2D Hybrid Lead Halide Perovskites. *J. Phys. Chem. C* **2017,** *121* (47), 26566-26574.

14. Tsai, H.; Asadpour, R.; Blancon, J.-C.; Stoumpos, C. C.; Even, J.; Ajayan, P. M.; Kanatzidis, M. G.; Alam, M. A.; Mohite, A. D.; Nie, W., Design principles for electronic charge transport in solution-processed vertically stacked 2D perovskite quantum wells. *Nat. Commun.* **2018,** *9* (1), 2130.

15. Wang, Z.; Lin, Q.; Chmiel, F. P.; Sakai, N.; Herz, L. M.; Snaith, H. J. Efficient ambient-air-stable solar cells with 2D–3D heterostructured butylammonium-caesium-formamidinium lead halide perovskites. *Nat. Energy* **2017,** *2* (9), 1-10.

16. Rodríguez-Romero, J.; Hames, B. C.; Mora-Seró, I.; Barea, E. M., Conjugated Organic Cations to Improve the Optoelectronic Properties of 2D/3D Perovskites. *ACS Energy Lett.* **2017,** *2* (9), 1969-1970.

17. Gharibzadeh, S.; Abdollahi Nejand, B.; Jakoby, M.; Abzieher, T.; Hauschild, D.; Moghadamzadeh, S.; Schwenzer, J. A.; Brenner, P.; Schmager, R.; Haghighirad, A. A., Weinhardt, L., Lemmer, U., Richards, B. S., Howard, I. A., Paetzold, U. W., Record open-circuit voltage wide-bandgap perovskite solar cells utilizing 2D/3D perovskite heterostructure. *Adv. Energy Mater.* **2019,** *9* (21), 1803699.

18. Rodríguez-Romero, J.; Clasen Hames, B.; Galar, P.; Fakharuddin, A.; Suarez, I.; Schmidt-Mende, L.; Martínez-Pastor, J. P.; Douhal, A.; Mora-Seró, I.; Barea, E. M., Tuning optical/electrical properties of 2D/3D perovskite by the inclusion of aromatic cation. *Phys. Chem. Chem. Phys.* **2018,** *20* (48), 30189-30199.

19. Nie, W.; Tsai, H.; Asadpour, R.; Blancon, J.-C.; Neukirch, A. J.; Gupta, G.; Crochet, J. J.; Chhowalla, M.; Tretiak, S.; Alam, M. A.; Wang, H.-L.; Mohite, A. D., High-efficiency solution-processed perovskite solar cells with millimeter-scale grains. *Science* **2015,** *347* (6221), 522-525.

20. Liao, Y.; Liu, H.; Zhou, W.; Yang, D.; Shang, Y.; Shi, Z.; Li, B.; Jiang, X.; Zhang, L.; Quan, L. N.; Quintero-Bermudez, R.; Sutherland, B. R.; Mi, Q.; Sargent, E. H.; Ning, Z., Highly Oriented Low-Dimensional Tin Halide Perovskites with Enhanced Stability and Photovoltaic Performance. *J. Am. Chem. Soc.* **2017,** *139* (19), 6693-6699.

21. Smith, I. C.; Hoke, E. T.; Solis-Ibarra, D.; McGehee, M. D.; Karunadasa, H. I., A Layered Hybrid Perovskite Solar-Cell Absorber with Enhanced Moisture Stability. *Angew. Chem. Int. Ed.* **2014,** *53* (42), 11232-11235.

22. Rodríguez-Romero, J.; Sanchez-Diaz, J.; Echeverría-Arrondo, C.; Masi, S.; Esparza, D.; Barea, E. M.; Mora-Seró, I., Widening the 2D/3D Perovskite Family for Efficient and Thermal-Resistant Solar Cells by the Use of Secondary Ammonium Cations. *ACS Energy Lett.* **2020,** *5* (4), 1013-1021.

23. Li, F.; Yang, L.; Cai, Z.; Wei, K.; Lin, F.; You, J.; Jiang, T.; Wang, Y.; Chen, X., Enhancing exciton binding energy and photoluminescence of formamidinium lead bromide by reducing its dimensions to 2D nanoplates for producing efficient light emitting diodes. *Nanoscale* **2018,** *10* (44), 20611-20617.

24. Mitzi, D. B.; Feild, C. A.; Harrison, W. T. A.; Guloy, A. M., Conducting tin halides with a layered organic-based perovskite structure. *Nature* **1994,** *369*, 467.

25. Mitzi, D. B.; Wang, S.; Feild, C. A.; Chess, C. A.; Guloy, A. M., Conducting Layered Organic-inorganic Halides Containing <110>-Oriented Perovskite Sheets. *Science* **1995,** *267* (5203), 1473-6.

26. Xu, Z.; Mitzi, D. B.; Medeiros, D. R., [(CH3)3NCH2CH2NH3]SnI4: a layered perovskite with quaternary/primary ammonium dications and short interlayer iodine-iodine contacts. *Inorg. Chem.* **2003,** *42* (5), 1400-2.

27. Stoumpos, C. C.; Cao, D. H.; Clark, D. J.; Young, J.; Rondinelli, J. M.; Jang, J. I.; Hupp, J. T.; Kanatzidis, M. G., Ruddlesden–Popper hybrid lead iodide perovskite 2D homologous semiconductors. *Chem. Mater.* **2016,** *28* (8), 2852-2867.

28. Stoumpos, C. C.; Soe, C. M. M.; Tsai, H.; Nie, W.; Blancon, J.-C.; Cao, D. H.; Liu, F.; Traoré, B.; Katan, C.; Even, J., Mohite, A. D., Kanatzidis, M. G., High members of the 2D Ruddlesden-Popper halide perovskites: synthesis, optical properties, and solar cells of (CH3 (CH2) 3NH3) 2 (CH3NH3) 4Pb5I16. *Chem* **2017,** *2* (3), 427-440.

29. Quan, L. N.; Yuan, M.; Comin, R.; Voznyy, O.; Beauregard, E. M.; Hoogland, S.; Buin, A.; Kirmani, A. R.; Zhao, K.; Amassian, A.; Kim, D. H.; Sargent, E. H., Ligand-Stabilized Reduced-Dimensionality Perovskites. *J. Am. Chem. Soc.* **2016,** *138* (8), 2649-55.

30. Wang, N.; Cheng, L.; Ge, R.; Zhang, S.; Miao, Y.; Zou, W.; Yi, C.; Sun, Y.; Cao, Y.; Yang, R., Wei, Y., Guo, Q., Ke, Y., Yu, M., Jin, Y., Liu, Y., Ding, Q., Di, D., Le, Y., Xing G., Tian, H., Jin, C., Gao, F., Friend, R. H., Wang, J., Huang, W.,

Perovskite light-emitting diodes based on solution-processed self-organized multiple quantum wells. *Nat. Photonics* **2016,** *10* (11), 699-704.

31. Proppe, A. H.; Elkins, M. H.; Voznyy, O.; Pensack, R. D.; Zapata, F.; Besteiro, L. V.; Quan, L. N.; Quintero-Bermudez, R.; Todorovic, P.; Kelley, S. O.; Govorov, A. O.; Gray, S. K.; Infante, I.; Sargent, E. H.; Scholes, G. D., Spectrally Resolved Ultrafast Exciton Transfer in Mixed Perovskite Quantum Wells. *J. Phys. Chem. Lett.* **2019,** *10* (3), 419-426.

32. Liang, C.; Gu, H.; Xia, Y.; Wang, Z.; Liu, X.; Xia, J.; Zuo, S.; Hu, Y.; Gao, X.; Hui, W.; Chao, L.; Niu, T.; Fang, M.; Lu, H.; Dong, H.; Yu, H.; Chen, S.; Ran, X.; Song, L.; Li, B.; Zhang, J.; Peng, Y.; Shao, G.; Wang, J.; Chen, Y.; Xing, G.; Huang, W., Two-dimensional Ruddlesden–Popper layered perovskite solar cells based on phase-pure thin films. *Nat. Energy* **2021,** *6* (1), 38-45.

33. Yan, K.; Long, M.; Zhang, T.; Wei, Z.; Chen, H.; Yang, S.; Xu, J., Hybrid Halide Perovskite Solar Cell Precursors: Colloidal Chemistry and Coordination Engineering behind Device Processing for High Efficiency. *J. Am. Chem. Soc.* **2015,** *137* (13), 4460-4468.

34. Yu, S.; Yan, Y.; Chen, Y.; Chábera, P.; Zheng, K.; Liang, Z., Enabling room-temperature processed highly efficient and stable 2D Ruddlesden–Popper perovskite solar cells with eliminated hysteresis by synergistic exploitation of additives and solvents. *J. Mater. Chem. A* **2019,** *7* (5), 2015-2021.

35. Provencher, S. W., CONTIN: A general purpose constrained regularization program for inverting noisy linear algebraic and integral equations. *Comput. Phys. Commun.* **1982,** *27* (3), 229-242.

36. Giannozzi, P.; Baroni, S.; Bonini, N.; Calandra, M.; Car, R.; Cavazzoni, C.; Ceresoli, D.; Chiarotti, G. L.; Cococcioni, M.; Dabo, I.; Dal Corso, A.; de Gironcoli, S.; Fabris, S.; Fratesi, G.; Gebauer, R.; Gerstmann, U.; Gougoussis, C.; Kokalj, A.; Lazzeri, M.; Martin-Samos, L.; Marzari, N.; Mauri, F.; Mazzarello, R.; Paolini, S.; Pasquarello, A.; Paulatto, L.; Sbraccia, C.; Scandolo, S.; Sclauzero, G.; Seitsonen, A. P.; Smogunov, A.; Umari, P.; Wentzcovitch, R. M., QUANTUM ESPRESSO: a modular and open-source software project for quantum simulations of materials. *J. Phys.-Condens. Mat.* **2009,** *21* (39), 395502.

37. Perdew, J. P.; Burke, K.; Ernzerhof, M., Generalized Gradient Approximation Made Simple. *Phys. Rev. Lett.* **1996,** *77* (18), 3865-3868.

38. Zhang, F.; Kim, D. H.; Lu, H.; Park, J.-S.; Larson, B. W.; Hu, J.; Gao, L.; Xiao, C.; Reid, O. G.; Chen, X.; Zhao, Q.; Ndione, P. F.; Berry, J. J.; You, W.; Walsh, A.; Beard, M. C.; Zhu, K., Enhanced Charge Transport in 2D Perovskites via Fluorination of Organic Cation. *J. Am. Chem. Soc.* **2019,** *141* (14), 5972-5979.

39. Li, X.; Hoffman, J. M.; Kanatzidis, M. G., The 2D Halide Perovskite Rulebook: How the Spacer Influences Everything from the Structure to Optoelectronic Device Efficiency. *Chem. Rev.* **2021,** *121* (4), 2230-2291.

40. García-Benito, I.; Quarti, C.; Queloz, V. I. E.; Orlandi, S.; Zimmermann, I.; Cavazzini, M.; Lesch, A.; Marras, S.; Beljonne, D.; Pozzi, G.; Nazeeruddin, M. K.; Grancini, G., Fashioning Fluorous Organic Spacers for Tunable and Stable Layered Hybrid Perovskites. *Chem. Mater.* **2018,** *30* (22), 8211-8220.

41. Cho, K. T.; Zhang, Y.; Orlandi, S.; Cavazzini, M.; Zimmermann, I.; Lesch, A.; Tabet, N.; Pozzi, G.; Grancini, G.; Nazeeruddin, M. K., Water-Repellent Low-Dimensional Fluorous Perovskite as Interfacial Coating for 20% Efficient Solar Cells. *Nano Lett.* **2018,** *18* (9), 5467-5474.

42. Hu, J.; Oswald, I. W. H.; Stuard, S. J.; Nahid, M. M.; Zhou, N.; Williams, O. F.; Guo, Z.; Yan, L.; Hu, H.; Chen, Z.; Xiao, X.; Lin, Y.; Yang, Z.; Huang, J.; Moran, A. M.; Ade, H.; Neilson, J. R.; You, W., Synthetic control over orientational degeneracy of spacer cations enhances solar cell efficiency in two-dimensional perovskites. *Nat. Commun.* **2019,** *10* (1), 1276.

43. Wang, L.; Zhou, Q.; Zhang, Z.; Li, W.; Wang, X.; Tian, Q.; Yu, X.; Sun, T.; Wu, J.; Zhang, B.; Gao, P., A guide to use fluorinated aromatic bulky cations for stable and high-performance 2D/3D perovskite solar cells: The more fluorination the better? *J. Energy Chem.* **2022,** *64*, 179-189.

44. Torres, A.; Rego, L. G. C., Surface Effects and Adsorption of Methoxy Anchors on Hybrid Lead Iodide Perovskites: Insights for Spiro-MeOTAD Attachment. *J. Phys. Chem. C* **2014,** *118* (46), 26947-26954.

45. Hu, H.; Morris, S. A.; Qiao, X.; Zhao, D.; Salim, T.; Chen, B.; Chia, E. E. M.; Lam, Y. M., Molecular engineering of two-dimensional hybrid perovskites with

broadband emission for white light-emitting diodes. *J. Mater. Chem. C* **2018,** *6* (38), 10301-10307.

46. de Holanda, M. S.; Szostak, R.; Marchezi, P. E.; Duarte, L. G. T. A.; Germino, J. C.; Atvars, T. D. Z.; Nogueira, A. F., In Situ 2D Perovskite Formation and the Impact of the 2D/3D Structures on Performance and Stability of Perovskite Solar Cells. *Sol. RRL* **2019,** *3* (9), 1900199.

47. Chirvony, V. S.; Suárez, I.; Rodríguez-Romero, J.; Vázquez-Cárdenas, R.; Sanchez-Diaz, J.; Molina-Sánchez, A.; Barea, E. M.; Mora-Seró, I.; Martínez-Pastor, J. P., Inhomogeneous Broadening of Photoluminescence Spectra and Kinetics of Nanometer-Thick (Phenethylammonium)2PbI4 Perovskite Thin Films: Implications for Optoelectronics. *ACS Appl. Nano Mater.* **2021,** *4* (6), 6170-6177.

48. Blancon, J. C.; Tsai, H.; Nie, W.; Stoumpos, C. C.; Pedesseau, L.; Katan, C.; Kepenekian, M.; Soe, C. M.; Appavoo, K.; Sfeir, M. Y.; Tretiak, S.; Ajayan, P. M.; Kanatzidis, M. G.; Even, J.; Crochet, J. J.; Mohite, A. D., Extremely efficient internal exciton dissociation through edge states in layered 2D perovskites. *Science* **2017,** *355* (6331), 1288-1292.

49. Yuan, M.; Quan, L. N.; Comin, R.; Walters, G.; Sabatini, R.; Voznyy, O.; Hoogland, S.; Zhao, Y.; Beauregard, E. M.; Kanjanaboos, P.; Lu, Z.; Kim, D. H.; Sargent, E. H., Perovskite energy funnels for efficient light-emitting diodes. *Nat. Nanotechnol.* **2016,** *11* (10), 872-877.

50. Proppe, A. H.; Quintero-Bermudez, R.; Tan, H.; Voznyy, O.; Kelley, S. O.; Sargent, E. H., Synthetic Control over Quantum Well Width Distribution and Carrier Migration in Low-Dimensional Perovskite Photovoltaics. *J. Am. Chem. Soc.* **2018,** *140* (8), 2890-2896.

51. Kong, L.; Zhang, X.; Li, Y.; Wang, H.; Jiang, Y.; Wang, S.; You, M.; Zhang, C.; Zhang, T.; Kershaw, S. V.; Zheng, W.; Yang, Y.; Lin, Q.; Yuan, M.; Rogach, A. L.; Yang, X., Smoothing the energy transfer pathway in quasi-2D perovskite films using methanesulfonate leads to highly efficient light-emitting devices. *Nat. Commun.* **2021,** *12* (1), 1246.

52. Li, W.; Fan, J.; Li, J.; Mai, Y.; Wang, L., Controllable Grain Morphology of Perovskite Absorber Film by Molecular Self-Assembly toward Efficient Solar Cell Exceeding 17%. *J. Am. Chem. Soc.* **2015,** *137* (32), 10399-10405.

53. Jung, M.; Ji, S.-G.; Kim, G.; Seok, S. I., Perovskite precursor solution chemistry: from fundamentals to photovoltaic applications. *Chem. Soc. Rev.* **2019,** *48* (7), 2011-2038.

54. Liu, C.; Cheng, Y.-B.; Ge, Z., Understanding of perovskite crystal growth and film formation in scalable deposition processes. *Chem. Soc. Rev.* **2020,** *49* (6), 1653-1687.

55. Zhang, Y.; Gao, P.; Oveisi, E.; Lee, Y.; Jeangros, Q.; Grancini, G.; Paek, S.; Feng, Y.; Nazeeruddin, M. K., PbI2–HMPA Complex Pretreatment for Highly Reproducible and Efficient CH3NH3PbI3 Perovskite Solar Cells. *J. Am. Chem. Soc.* **2016,** *138* (43), 14380-14387.

56. Sun, B.; Wang, W.; Lu, H.; Chao, L.; Gu, H.; Tao, L.; Hu, J.; Li, B.; Zong, X.; Shi, W.; Ran, X.; Zhang, H.; Xia, Y.; Li, P.; Chen, Y., Tuning the Interactions of Methylammonium Acetate with Acetonitrile to Create Efficient Perovskite Solar Cells. *J. Phys. Chem. C* **2021,** *125* (12), 6555-6563.

57. Hamill, J. C.; Schwartz, J.; Loo, Y.-L., Influence of Solvent Coordination on Hybrid Organic–Inorganic Perovskite Formation. *ACS Energy Lett.* **2018,** *3* (1), 92-97.

58. Yuan, F.; Zheng, X.; Johnston, A.; Wang, Y.-K.; Zhou, C.; Dong, Y.; Chen, B.; Chen, H.; Fan, J. Z.; Sharma, G.; Li, P.; Gao, Y.; Voznyy, O.; Kung, H.-T.; Lu, Z.-H.; Bakr, O. M.; Sargent, E. H., Color-pure red light-emitting diodes based on two-dimensional lead-free perovskites. *Sci. Adv.* **2020,** *6* (42), eabb0253.

59. Kikuchi, K.; Takeoka, Y.; Rikukawa, M.; Sanui, K., Structure and optical properties of lead iodide based two-dimensional perovskite compounds containing fluorophenethylamines. *Curr. Appl. Phys.* **2004,** *4* (6), 599-602.

TOC Graphic

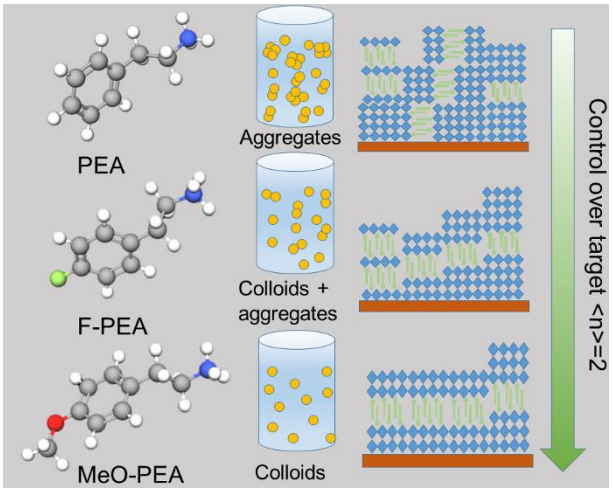
PEA
F-PEA
MeO-PEA
Aggregates
Colloids +
aggregates
Colloids
Control over target <n>=2